

# ALOcc: Adaptive Lifting-based 3D Semantic Occupancy and Cost Volume-based Flow Prediction

Dubing Chen<sup>1</sup>, Jin Fang<sup>1</sup>, Wencheng Han<sup>1</sup>, Xinjing Cheng,  
Junbo Yin<sup>2</sup>, Chenzhong Xu<sup>1</sup>, Fahad Shahbaz Khan<sup>3,4</sup>, Jianbing Shen<sup>1\*</sup>

<sup>1</sup>SKL-IOTSC, CIS, University of Macau

<sup>2</sup>CMESE Division, King Abdullah University of Science and Technology (KAUST)

<sup>3</sup>Mohamed bin Zayed University of Artificial Intelligence <sup>4</sup>Linköping University

{dobbin.chen, fangjin19900820, wencheng256, cnorbot}@gmail.com

junbo.yin@kaust.edu.sa, czxu@um.edu.mo, fahad.khan@mbzuai.ac.ae, jianbingshen@um.edu.mo

<https://github.com/cdb342/ALOcc>

## Abstract

Vision-based semantic occupancy and flow prediction plays a crucial role in providing spatiotemporal cues for real-world tasks, such as autonomous driving. Existing methods prioritize higher accuracy to cater to the demands of these tasks. In this work, we strive to improve performance by introducing a series of targeted improvements for 3D semantic occupancy prediction and flow estimation. First, we introduce an occlusion-aware adaptive lifting mechanism with a depth denoising technique to improve the robustness of 2D-to-3D feature transformation and reduce the reliance on depth priors. Second, we strengthen the semantic consistency between 3D features and their original 2D modalities by utilizing shared semantic prototypes to jointly constrain both 2D and 3D features. This is complemented by confidence- and category-based sampling strategies to tackle long-tail challenges in 3D space. To alleviate the feature encoding burden in the joint prediction of semantics and flow, we propose a BEV cost volume-based prediction method that links flow and semantic features through a cost volume and employs a classification-regression supervision scheme to address the varying flow scales in dynamic scenes. Our purely convolutional architecture framework, named ALOcc, achieves an optimal tradeoff between speed and accuracy achieving state-of-the-art results on multiple benchmarks. On Occ3D and training without the camera visible mask, our ALOcc achieves an absolute gain of 2.5% in terms of RayIoU while operating at a comparable speed compared to the state-of-the-art, using the same input size (256×704) and ResNet-50 backbone. Our method also achieves **2nd place in the CVPR24 Occupancy and Flow Prediction Competition**.

\* Corresponding author: Jianbing Shen

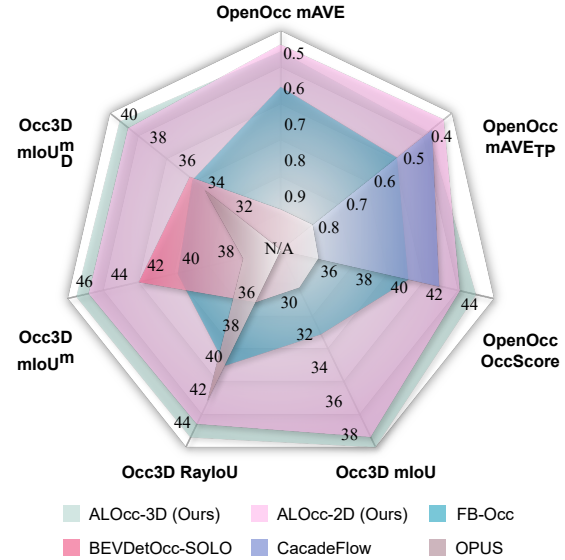


Figure 1. Semantic occupancy and flow prediction results of our ALOcc. ALOcc outperforms previous SOTAs across various benchmarks and metrics, demonstrating strong performance. The input image size and backbone are standardized to 256 × 704 and ResNet50, respectively.

## 1. Introduction

Accurate prediction of 3D semantic occupancy is vital for the effectiveness of perception systems, with widespread applications in autonomous driving, robotics, and virtual reality [11, 31, 38, 39, 41, 45]. Modeling both static and dynamic objects as 3D semantic grids offers multiple advantages. It provides a regularized representation of scene semantics, a finer granularity, and a more generalized form than traditional bounding boxes [10, 17, 19]. In recent years, the prediction of semantic occupancy and flow grid

maps solely from surround-view camera sensor data has received notable attention [11, 38, 39].

Vision-based 3D semantic occupancy prediction strives to infer regularized 3D scene semantics from 2D inputs. The task introduces an additional 2D-to-3D reconstruction, which is inherently an ill-posed problem. The challenges are two-fold. Firstly, the challenge is to accurately propagate 2D semantic signals to their correct 3D positions while predicting semantics accurately. Secondly, conducting computations on 3D data consumes substantial computational resources, which is particularly challenging for real-time tasks, such as autonomous driving. We are highly focused on the 2D-to-3D view transformation and the decoding of occupancy and flow. We examine two existing 2D-to-3D view transformation methods: depth-based lift-splat-shoot (LSS) [10, 17, 36] and 2D-3D cross attention [19, 21]. The former actively transmits 2D information to 3D by explicitly predicting 2.5D structural information (*i.e.*, depth), while the latter passively and adaptively transfers 2D information to 3D through cross attention with 3D queries. However, the depth-based LSS approach has several inherent problems, such as the strong depth inductive bias in the network. This will cause the network to get stuck in local optima due to early inaccurate depth estimations. It restricts signal propagation to occluded areas. Additionally, ray-based mapping in LSS tends to produce features with low spatial densities at far distances [21], impeding 3D feature learning for distant objects. Conversely, cross-attention does not evolve explicit structural information.

To address these challenges, we design an occlusion-aware adaptive lifting method that constructs transfer probabilities from surface to occluded and sparse locations based on explicit depth probabilities. This is inspired by human perception, where we can infer the shape and extent of occluded objects from partial views. In the occupancy decoder, we introduce a semantic enhancing method that correlates 3D and 2D features using a shared semantic prototype set. We predefine per-class semantic prototypes to aggregate class semantics from both 3D and 2D features. It helps transfer inter-class semantic relationships from original 2D signals to 3D and improves 3D semantic representation learning. We then calculate per-class segmentation masks using these prototypes. To address the long-tail problem in scenes, each prototype is trained only when the corresponding class is present in the scene. Additionally, we introduce a sampling technique based on uncertainty and class priors. We sample hard voxels based on class statistics and per-voxel prediction uncertainty. The training is only conducted on the sampled voxels.

Furthermore, we propose a new BEV-based cost volume method for occupancy flow prediction. A key challenge in this task is that jointly predicting semantics and flow imposes two types of representational pressure on the features.

To alleviate this pressure, we aggregate voxel features from multiple height levels above the ground into a BEV representation, creating a cost volume referenced to historical BEV features. Utilizing both the cost volume and voxel features for flow estimation allows voxel features to prioritize occupancy semantic information, thus mitigating multi-task prediction constraints. Additionally, we propose a hybrid classification-regression technique for flow prediction, enhancing the model’s adaptability to varied flow scales. As shown in Fig. 1, our method consistently outperforms existing approaches, establishing new state-of-the-art performance on multiple semantic occupancy and flow prediction benchmarks. Moreover, we propose ALOcc with multiple model variants through techniques like spatial compression. Our approach achieves superior performance while maintaining competitive computational efficiency. This establishes a favorable balance between model performance and computational cost, which is particularly beneficial for real-time applications such as autonomous driving.

In summary, our main contributions are:

- We introduce a 2D-to-3D adaptive lifting method that transforms 2D signals to occluded and sparse areas via adaptive weight adjustment while incorporating depth denoising to prevent convergence to local optima.
- We are the first to present a BEV-based cost volume method for occupancy flow prediction, alleviating feature coding burden in multi-task settings and enhancing flow prediction with combined classification and regression.
- We proposed shared semantic prototypes to transfer inter-class relationships from 2D to 3D, mitigating the class imbalance problem through selective prototype training and uncertainty-aware sampling.
- Comprehensive evaluations across multiple semantic occupancy and flow prediction benchmarks demonstrate consistent improvements over current SOTAs. We provide multiple model variants, with our real-time version outperforming existing real-time approaches.

## 2. Related Work

**Semantic Scene Completion (SSC)** [5, 15, 18, 26, 50] endeavors to reconstruct and semantically complete 3D scenes from given inputs. Early research focused on indoor scenes [5, 15, 26], predicting occupancy and semantic labels in limited scenarios. Subsequent studies gradually shifted attention to complex outdoor environments, especially within driving contexts [1, 4]. The essence of SSC is its capacity to perceive the unobserved, filling gaps in partial observations with precise semantic insight. Recent methodologies, such as VoxFormer [18], adopt a two-stage approach that initially predicts occupancy, followed by semantic prediction of the occupied segments. OccFormer [50] introduces a dual-path Transformer submodule for 3D encoding and employs a query-based segmentation method [6].

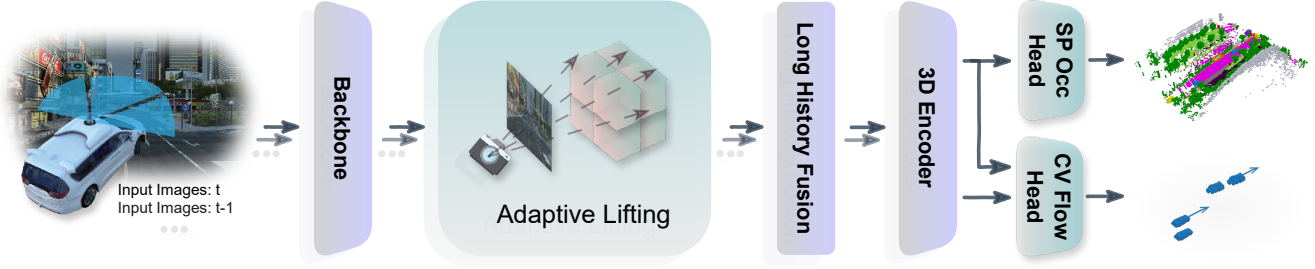


Figure 2. Overall Framework of the proposed ALOcc. The image features are converted to 3D space by adaptive lifting and then encoded by a 3D encoder along with the history frames. The resulting volume features are then decoded by different task heads.

The domain of **Vision-based 3D Occupancy Prediction** [11, 38, 39, 41] aligns closely with SSC but emphasizes multi-perspective joint perception, essential for autonomous navigation. Occupancy prediction demands the delineation of intricate 3D scenes into fine-grained elements to adeptly navigate dynamic driving contexts. Initial efforts like TPVFormer [11] employed sparse point clouds for supervision, utilizing spatial attention for granular predictions. Subsequent works such as OccNet [39], SurroundOcc [43], Occ3D [38], and OpenOccupancy [41] have constructed more dense occupancy annotations based on temporal information and instance-level labeling. Some studies [20, 32] have drawn from explicit geometric prediction methods [10, 17, 20] to facilitate 2D-to-3D view transformation. With computational efficiency in mind, Liu et al. [24, 24], Lu et al. [30], Wang et al. [40, 42] has focused on the sparsification of 3D representations and computations. Studies like [12, 27, 34, 48] have explored Nerf-based rendering for supervision-light approaches. Liu et al. [24] explored a new metric, RayIoU, to address the limitations of previous measures. Furthermore, recent research [16, 27, 39] introduced 3D occupancy flow prediction, which focuses on per-voxel dynamics, extending the capability of 3D scene understanding. However, previous research lacked a cohesive evaluation framework, often conducting experiments on isolated benchmarks (such as Occ3D [38] or OpenOcc [39]) or comparing performance using single metrics (like mIoU or RayIoU). In this work, we present a unified approach that excels in both semantic occupancy prediction and occupancy flow prediction tasks, validated through comprehensive evaluation metrics.

### 3. The Proposed Method

Our research focuses on vision-based 3D semantic occupancy and flow prediction. Given  $N$  input images  $\{\mathbf{I}^i \in \mathbb{R}^{H \times W \times 3}\}_{i=1}^N$ , the goal is to predict the 3D semantic occupancy grid and the 3D occupancy flow grid, supervised by the corresponding groundtruth  $\mathbf{O}_s \in \mathbb{R}^{X \times Y \times Z}$  and  $\mathbf{O}_f \in \mathbb{R}^{X \times Y \times Z \times 2}$ . Each value in  $\mathbf{O}_s$  identifies the class of its corresponding spatial position, including *empty* (indicat-

ing unoccupied space) and semantic classes such as *pedestrian* and *car*. Each voxel in the flow grid  $\mathbf{O}_f$  contains a 2D flow vector specifying movement in the  $x$  and  $y$  directions. Fig. 2 presents a schematic view of our approach. Initially, 2D features are extracted from surrounding images, which are subsequently transformed into 3D space by adaptive lifting. The lifted features are encoded within the 3D space, together with historical frame data. The encoded volume features are then decoded by various task heads to predict the 3D semantic occupancy and flow grids.

Overall, Sec. 3.2 introduces the occlusion-aware adaptive lifting technique that enhances 2D-to-3D view transformation. Sec. 3.3 details our semantic prototype-based occupancy prediction head which strengthens the 2D-3D semantic alignment and mitigates the long-tail problem. Sec. 3.4 discusses the BEV cost volume approach and a new regression-classification strategy to enhance occupancy flow predictions.

#### 3.1. Revisiting Depth-based LSS

As the core module of vision-based occupancy prediction, the 2D-to-3D view transformation process is formulated as:

$$\mathbf{V}_f = \mathbf{M}_T \cdot \text{cat}\{\mathbf{I}_f^i\}_{i=1}^N, \quad (1)$$

where  $\mathbf{I}_f^i$  and  $\mathbf{V}_f$  represent the image features and the lifted features.  $\text{cat}\{\cdot\}$  signifies the concatenation operation, and we omit the flattening and reshaping operations here.

Depth-based LSS initializes  $\mathbf{M}_T$  as a zero matrix and populates it with image depth probabilities. For each pixel  $\mathbf{x}^{(u,v)}$ , depth is predicted as occupancy probability over discretized bins along the camera sightline:  $\{P(o_d^i|\mathbf{x})\}_{i=1}^D$ . The coordinate projection function  $R(\cdot)$  maps 3D coordinates  $(u, v, d)$  from the image coordinate system (ICS) to the voxel coordinate system (VCS):  $(x, y, z) = R(u, v, d)$ . Each depth probability is assigned to  $\mathbf{M}_T$  at the row index corresponding to the rounded voxel coordinate  $[(x, y, z)]$  and the column index corresponding to  $(u, v)$ . Due to the sparsity of  $\mathbf{M}_T$ , this process is typically implemented with sparse operations *e.g.*, `sparse_coo_tensor` in PyTorch or BEVPool [10, 36].

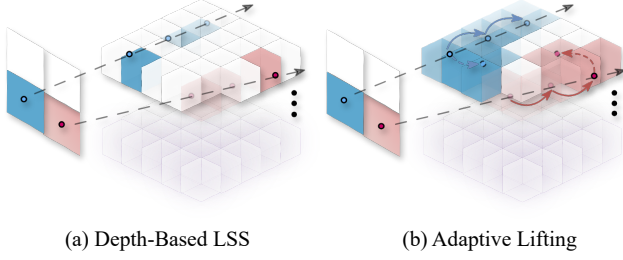


Figure 3. Comparison between (a) Depth-based LSS and (b) Our occlusion-aware adaptive lifting. The dotted line represents the camera sightline, and opacity indicates the weight of mapping 2D features to 3D voxels, with higher opacity indicating larger weights.

### 3.2. Occlusion-Aware Adaptive Lifting

We enhance depth-based LSS by introducing probability transfer from surface to occluded areas. We first replace the hard rounding-based filling strategy in Sec. 3.1 with a probability-based soft filling approach. As detailed in Fig. 3, we use trilinear interpolation to diffuse the probability of a point  $(x, y, z)$  over its eight neighboring points in VCS. The interpolation calculates eight probability values:

$$p_i = (1 - |x - \hat{x}_i|) \cdot (1 - |y - \hat{y}_i|) \cdot (1 - |z - \hat{z}_i|), \quad (2)$$

where  $\{(\hat{x}_i, \hat{y}_i, \hat{z}_i)\}_{i=1}^8$  are the neighboring voxel center coordinates. We then fill  $\mathbf{M}_T$  with  $p_i \cdot P_{x,y,z}^o$ , indexing the column with the corresponding ICS coordinate and the row with  $(\hat{x}_i, \hat{y}_i, \hat{z}_i)$ . This approach distributes depth probability  $P_{x,y,z}^o$  based on distance, making the 2D-to-3D mapping differentiable w.r.t. coordinates.

Depth-based LSS methods excel by guiding the 2D-to-3D feature transformation through explicit depth probability modeling. However, the target of depth estimation follows a  $\delta$  distribution, which causes most of the weights to concentrate on surface points. As a result, occluded areas receive significantly lower weights, leading to an inductive bias that limits the model’s ability to capture information from these regions. We aim to bridge this gap between visible and occluded parts during view transformation. Specifically, we address two types of occlusion: 1) the occlusion within the same object, and 2) the occlusion between different objects. For both, we construct a probability transfer matrix from visible to occluded parts. For the former type of occlusion, we design conditional probabilities to transfer surface probabilities to occluded length probabilities. Given the discrete depth probabilities  $\{P(o_d^i)\}_{i=1}^D$  of pixel point  $\mathbf{x}$ , we employ identical bin divisions for discretized occluded length prediction. We introduce a Bayes conditional probability  $P(o_l|o_d)$  to convert discrete depth probability  $P(o_d)$

into discrete occluded length probability  $P(o_l)$ :

$$P(o_l^j) = \sum_{i=1}^D P(o_l^j|o_d^i) \cdot P(o_d^i), \quad j = 1, \dots, D. \quad (3)$$

To determine  $P(o_l^j|o_d^i)$ , we consider the physical meaning of depth: if the camera sightline reaches point  $i$ , it indicates that all points at shallower depths (*i.e.*, with indices smaller than  $i$ ) are empty. Therefore, we only need to estimate the conditional probability for depth  $d^i$  to positions with larger depth.  $P(o_l^j|o_d^i)$  is modeled as:

$$P(o_l^j|o_d^i) = \begin{cases} 0, & \text{if } j < i \\ 1, & \text{if } j = i \\ f_h(\mathbf{x}, j - i), & \text{if } j > i. \end{cases} \quad (4)$$

where  $f_h(\mathbf{x}, j - i)$  represents the likelihood of bin  $j$  being occupied if bin  $i$  corresponds to the surface point. For each pixel point  $\mathbf{x}$ , we compute  $(D - 1)$  discrete probabilities encompassing all relative positions between  $i$  and  $j$ . In practice, the transformation from depth to occluded length probabilities is implemented by multiplying the depth probabilities by the casual conditional probability matrix.

For inter-object occlusion, we design a probability transfer matrix to propagate occupation probabilities to surrounding points. For each point  $(u, v, d^i)$ , we estimate multiple offsets  $(\Delta u_k, \Delta v_k)$  and corresponding transfer weights  $w_k$  based on its feature  $\mathbf{x}$ . New surrounding points  $(u + \Delta u_k, v + \Delta v_k, d^i; w_k \cdot P(o_l^i))$  are then incorporated into  $\mathbf{M}_T$  via soft filling, and can be optimized during training. For computation efficiency, we apply this transfer only to the  $k$  points with the top depth probabilities.

The predominant role of depth probabilities in 2D-to-3D semantic transformation can lead to suboptimal model convergence due to initial inaccurate depth estimations. To mitigate this, we introduce a denoising operation analogous to query denoising in object detection algorithms [8, 14, 49]. This approach utilizes groundtruth depth probabilities to guide early model training. We employ a weighted average of groundtruth and predicted depths to guide the adaptive lifting process in training. The weight of ground truth depth is initialized with 1 and gradually reduced to 0 following a cosine annealing strategy. This can be formulated as:

$$P(o_d) = \frac{1 + \cos(\frac{\pi t}{T})}{2} \cdot P_{gt}(o_d) + \frac{1 - \cos(\frac{\pi t}{T})}{2} \cdot P_{pred}(o_d), \quad (5)$$

where  $P(o_d)$  is the final depth probability used for adaptive lifting.  $P_{gt}(o_d)$  and  $P_{pred}(o_d)$  are ground truth and predicted depth probabilities, respectively.  $t$  is the current training step, and  $T$  is the total number of annealing steps. During test,  $P(o_d) = P_{pred}(o_d)$ .



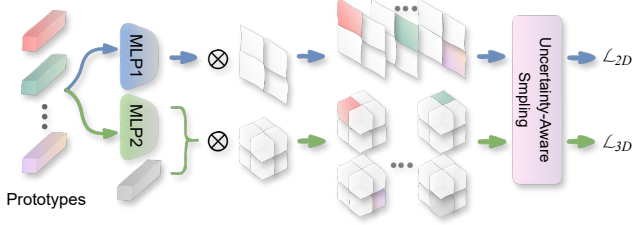


Figure 4. Semantic Prototype-Based Occupancy Head. Shared semantic prototypes calculate segmentation logits for both 2D and 3D features. Training is conducted only on the top  $K$  voxels (or pixels) sampled based on logits uncertainty.

### 3.3. Semantic Prototype-based Occupancy Head

After the 2D-to-3D feature transformation, we enhance semantic alignment between 2D and 3D features using shared prototypes. As illustrated in Fig. 4, we initialize a semantic prototype for each class, which simultaneously serves as the class weights in the loss calculations for both 2D and 3D features. This shared prototype approach creates a shortcut linking 2D and 3D semantics, promoting consistent feature representation across dimensions.

Given the prototypes for each class, an intuitive way to decode the semantic occupancy is to calculate the similarity between voxel features and prototypes, followed by cross-entropy supervision. However, this approach is suboptimal due to the highly skewed distribution of semantic categories in driving scenes. To address this imbalance, we propose a prototype-independent loss that considers only the classes present in the groundtruth occupancy map of each scene.

We extract prototypes (including an embedding for the *empty* class) for all existing semantic categories by groundtruth and compute inner products between these prototypes and 3D features to generate class masks. To further enhance training for tail categories, we employ an uncertainty and class prior-based sampling technique [6, 13, 50]. We use a per-prototype logit map derived from inner products as a measure of per-voxel uncertainty. This uncertainty and the class prior form a multinomial distribution. We then sample  $K$  voxels from the entire occupancy map according to this distribution. The loss is only calculated on the sampled points. The final 3D perception loss is formulated as a combination of binary cross-entropy and dice loss:

$$\mathcal{L}_{3D} = \alpha \mathcal{L}_{Dice} + \beta \mathcal{L}_{bce}, \quad (6)$$

where  $\alpha, \beta$  are balancing coefficients, and  $\mathcal{L}_{Dice}$  and  $\mathcal{L}_{bce}$  represent dice loss and binary cross-entropy loss, respectively. Each category mask is predicted independently, ensuring that abundant categories do not overshadow minority classes.  $\mathcal{L}_{2D}$  applies similar supervision in 2D space, using both dice loss and binary cross-entropy loss to guide the 2D feature map. Ultimately, each voxel’s predicted category is

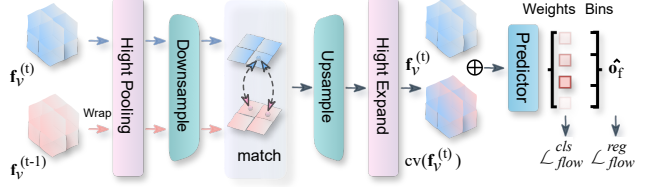


Figure 5. Illustration of the Flow Head. The cost volume is generated from downsampled BEV features and used to predict bin probabilities along with volume features. Final flow values are computed as a weighted sum of the bin center values.

determined as the one with the highest response to the semantic prototype or empty embedding:

$$\mathbf{o}_v = \arg \max_c (\text{MLP}(P_c) \cdot \mathbf{f}_v), \quad (7)$$

where  $\mathbf{f}_v$  represents the features of the voxel,  $P_c$  denotes the prototype of category  $c$  or the free embedding, and MLP further encodes  $P_c$ .

### 3.4. BEV Cost Volume-based Occupancy Flow Prediction

As shown in Fig. 2, we decode the occupancy flow also from the encoded volume features. Basically, a flow network  $f_{flow}$  predicts the occupancy flow as

$$\hat{\mathbf{o}}_f = f_{flow}(\mathbf{f}_v), \quad (8)$$

where we supervise against the groundtruth flow  $\mathbf{o}_f$  by minimizing the L2 loss and maximizing the cosine similarity:

$$\mathcal{L}_{flow}^{reg} = \|\hat{\mathbf{o}}_f - \mathbf{o}_f\|_2^2 - \frac{\hat{\mathbf{o}}_f^i \cdot \mathbf{o}_f^i}{\|\hat{\mathbf{o}}_f^i\|_2 \cdot \|\mathbf{o}_f^i\|_2}, \quad (9)$$

where the L2 loss ensures magnitude accuracy, while cosine similarity guarantees the directional precision. Simultaneously predicting semantic occupancy and flow requires both semantic and motion information, increasing the pressure on feature encoding. Therefore, we propose constructing a flow prior (*i.e.*, BEV cost volume) based on cross-frame semantic information. Specifically, we average the volume features from 0 to 4m in height to create a foreground-focused BEV feature, as shown in Fig. 5. We downsample the BEV feature to increase the receptive field while reducing computational overhead. We then wrap the previous frame’s BEV feature to the current frame’s coordinate system using camera parameters and match it with current frame features at multiple hypothetical points around each point. The cost volume is constructed by calculating the cosine similarity between each pair of features:

$$cv(\mathbf{f}_v^{(t)}, i) = \frac{\mathbf{f}_v^{(t)} \cdot \text{wrap}(\mathbf{f}_v^{(t-1)}(\Delta p_i))}{\|\mathbf{f}_v^{(t)}\|_2 \cdot \|\text{wrap}(\mathbf{f}_v^{(t-1)}(\Delta p_i))\|_2}, \quad (10)$$

where  $\mathbf{f}_v^{(t)}$  is the BEV feature of the current frame,  $\text{wrap}(\mathbf{f}_v^{(t-1)})$  is the BEV feature of the previous frame warped to the current frame’s coordinate system, and  $\Delta p_i$  denotes the predefined hypothetic points. We omit the post-hoc upsampling and expanding operations, as shown in Fig. 5. The cost volume is then concatenated with the current frame’s BEV feature, and Eq. (8) can be rewritten as:

$$\hat{\mathbf{o}}_{\mathbf{f}} = f_{\text{flow}}(\text{cat}(\mathbf{f}_v^{(t)}, \text{cv}(\mathbf{f}_v^{(t)}))). \quad (11)$$

The cost volume-based flow prediction method calculates flow by semantically matching features with those at different positions in the previous frame, alleviating the representational burden of encoding both semantics and motion. Notably, it reuses cached volume features from the previous frame, avoiding the need for a second inference.

To improve our model’s capability to predict flow values across various scales, we present a hybrid method by incorporating regression and classification [2, 22]. We divide the flow values into multiple bins based on the maximum and minimum flow values derived from the training set. Our flow head predicts the likelihood of the flow falling into each bin. The continuous flow prediction is formulated as a weighted sum of the bin center values:

$$\hat{\mathbf{o}}_{\mathbf{f}} = \sum_{i=1}^{N_b} p_b^i \cdot \mathbf{b}^i, \quad (12)$$

where  $p_b^i$  is the predicted probability for the  $i$ -th bin,  $\mathbf{b}^i$  is the flow value corresponding to the  $i$ -th bin, and  $N_b$  is the total number of bins.

Based on the regression supervision loss in Eq. (9), we introduce an additional classification loss based on the ground truth bin index:

$$\mathcal{L}_{\text{flow}}^{\text{cls}} = - \sum_{i=1}^{N_b} \mathbb{1}(\text{Index}[\mathbf{o}_{\mathbf{f}}; \mathbf{b}] = \mathbf{b}^i) \log(p_b^i), \quad (13)$$

where  $\mathbb{1}(\cdot)$  is the indicator function and  $\text{Index}[\mathbf{o}_{\mathbf{f}}; \mathbf{b}]$  denotes the index of groundtruth  $\mathbf{o}_{\mathbf{f}}$  in the predefined bins. The final occupancy flow loss is:

$$\mathcal{L}_{\text{flow}} = \mathcal{L}_{\text{flow}}^{\text{reg}} + \mathcal{L}_{\text{flow}}^{\text{cls}} \quad (14)$$

### 3.5. Training Objective

The overall objective for training the semantic occupancy and flow network can be summarized as follows:

$$\mathcal{L}_{\text{total}} = \mathcal{L}_{3D} + \mathcal{L}_{2D} + \mathcal{L}_{\text{flow}} + \mathcal{L}_{\text{depth}}, \quad (15)$$

where  $\mathcal{L}_{\text{depth}}$  is the depth supervision loss.

## 4. Experiment

### 4.1. Experimental Setup

**Dataset.** We employ the NuScenes dataset [3], specifically designed for a variety of 3D perception tasks in autonomous driving research. It contains 700 training, 150 validation, and 150 test scenes. Occ3D [38] and OpenOcc [39] add voxel-wise annotations to NuScenes, spanning a range of  $-40m$  to  $40m$  on the X and Y axes, and  $-1m$  to  $5.4m$  on the Z axis. The voxel resolution is  $0.4m$  in all dimensions. Occ3D provides 18 semantic categories, including 17 object classes and one *empty* class that denotes unoccupied spaces. OpenOcc offers per-voxel motion flow for X and Y coordinates and 17 semantic categories, with one fewer category (“others”) compared to Occ3D.

**Benchmarks.** We evaluate our model on three benchmarks: *i) 3D semantic occupancy prediction with mask.* This benchmark emphasizes the prediction of observed regions. Following PanoOcc [42], OSP [37], FB-Occ [20] and *etc.*, we train on camera-visible areas using the mask provided by Occ3D. We assess mIoU for 17 semantic categories. Since self-driving tasks focus more on dynamic categories, we additionally report mIoU<sub>D</sub> for 8 dynamic foreground categories. *ii) 3D semantic occupancy prediction without mask.* This benchmark emphasizes the simultaneous prediction of both observed and occluded regions. Following SparseOcc [24], we train on Occ3D without using the camera visible mask. We calculate mIoU and RayIoU for 17 semantic categories. *iii) 3D semantic occupancy and flow prediction.* This benchmark highlights flow prediction. Following [24, 39], We evaluate it on OpenOcc. We report RayIoU for 16 semantic categories and mAVE<sub>TP</sub> for flow metrics in true positive areas. Their weighted average is denoted as Occ Score. In particular, we observed that mAVE<sub>TP</sub> exhibits a strong dependence on semantic occupancy prediction, resulting in suboptimal convergence across epochs. Therefore, we additionally employ per-voxel mAVE as a supplementary metric.

**Implementation Details.** For a fair comparison, we employ a ResNet-50 [7] backbone and an image size of  $256 \times 704$  for most experiments. We also use a Swin-Transformer Base [28] model and image size of  $512 \times 1408$  for scaling-up experiments in Tab. 1. We adopt the same method for depth estimation as used in [10, 21]. The voxel size is set to  $200 \times 200 \times 16$  with a feature dimension of 32 for our default 3D model. The voxel size is set to  $200 \times 200 \times 1$  with a feature dimension of 80 for our default 2D model. We follow [21, 35] to adopt 16 history frames for temporal fusion. CBGS [35] is used. We use the same image and BEV augmentation strategies as BEVDet [10]. The semantic occupancy experiments are trained on a global batch size of 16 with 12 epochs of training, while the occupancy and flow experiments are trained longer up to 18 epochs.

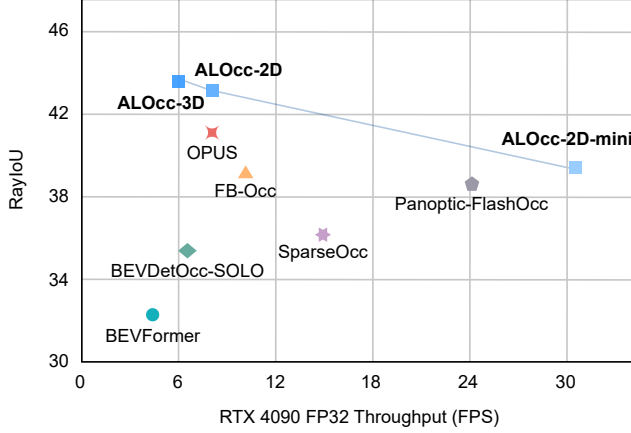


Figure 6. Speed/accuracy trade-off of our method. We benchmark RayIoU and speed on Occ3D using one RTX 4090 GPU with a batch size of 1. All the methods are tested using a ResNet-50 backbone and  $256 \times 704$  input size except for BEVFormer.

AdamW is employed as the optimizer [29] with a learning rate of  $2 \times 10^{-4}$ . Following Mask2Former, the loss weight  $\alpha$  and  $\beta$  are set to 5 and 20, respectively.

## 4.2. Accuracy/Speed Trade-off Evaluation

To evaluate ALOcc’s deployment capabilities, we analyze the speed-accuracy trade-off across multiple model variants. As shown in Fig. 6, we offer multiple model versions that achieve an excellent balance between accuracy and computational efficiency. Compared to ALOcc-3D, ALOcc-2D and ALOcc-2D-mini employ spatial compression techniques similar to FlashOcc [46], utilizing height compression and 2D convolutions for volume feature encoding. ALOcc-2D-mini uses monocular depth estimation, while others employ stereo depth estimation. ALOcc-2D-mini also employs a smaller channel size. Our results show ALOcc-3D and ALOcc-2D surpass SOTAs with higher speeds, and ALOcc-2D-mini achieves real-time inference while maintaining near SOTA performance.

## 4.3. Comparison with SOTAs

We compare our method with the current SOTAs on the Occ3D and OpenOcc datasets, with results summarized in Tab. 1, Tab. 2, and Tab. 3. The default ALOcc-2D model applies 2D convolutions for height-compressed volume encoding, using a channel number of 80. The default ALOcc-3D model uses 3D convolutions to encode the full 3D volume, with a channel number of 32. All results are presented without any post-processing like test-time augmentation.

**3D Semantic Occupancy Prediction with Mask.** As shown in Tab. 1, we compare our performance with the current SOTAs on Occ3D, focusing on training with the camera visible mask. This benchmark emphasizes the prediction of the camera-visible regions of the scene, which primar-

Method	Backbone	Input Size	mIoU <sub>D</sub> <sup>m</sup>	mIoU <sup>m</sup>	FPS
BEVDetOcc-SOLO [10]	ResNet-50	$256 \times 704$	34.4	41.9	6.5
UniOcc [33]	ResNet-50	$256 \times 704$	-	39.7	-
FB-Occ [20]	ResNet-50	$256 \times 704$	34.2	39.8	10.3
SurroundSDF [25]	ResNet-50	$256 \times 704$	36.2	42.4	-
FlashOcc [46]	ResNet-50	$256 \times 704$	24.7	32.0	29.6
COTR [32]	ResNet-50	$256 \times 704$	38.6	44.5	0.5
HyDRa* [44]	ResNet-50	$256 \times 704$	-	44.4	-
ViewFormer [16]	ResNet-50	$256 \times 704$	35.0	41.9	-
OPUS [40]	ResNet-50	$256 \times 704$	33.3	36.2	8.2
<b>ALOcc-2D-mini</b>	ResNet-50	$256 \times 704$	35.4	41.4	30.5
<b>ALOcc-2D</b>	ResNet-50	$256 \times 704$	38.7 $\uparrow 0.1$	44.8 $\uparrow 0.3$	8.2
<b>ALOcc-3D</b>	ResNet-50	$256 \times 704$	<b>39.3</b> $\uparrow 0.7$	<b>45.5</b> $\uparrow 1.0$	6.0
BEVFormer [19]	ResNet-101	$900 \times 1600$	37.2	39.2	4.4
VoxFormer [18]	ResNet-101	$900 \times 1600$	-	40.7	-
SurroundOcc [43]	ResNet-50	$900 \times 1600$	31.2	37.2	-
FastOcc [9]	ResNet-101	$640 \times 1600$	34.5	39.2	-
PanoOcc [42]	ResNet-101	$640 \times 1600$	37.3	42.1	-
OSP [37]	ResNet-101	$900 \times 1600$	37.0	41.2	-
BEVDetOcc [10]	Swin-Base	$512 \times 1408$	36.9	42.0	1.1
COTR [32]	Swin-Base	$512 \times 1408$	41.3	46.2	-
<b>ALOcc-2D</b>	Swin-Base	$512 \times 1408$	44.5 $\uparrow 3.2$	49.3 $\uparrow 3.1$	1.8
<b>ALOcc-3D</b>	Swin-Base	$512 \times 1408$	<b>46.1</b> $\uparrow 4.8$	<b>50.6</b> $\uparrow 4.4$	1.5

Table 1. 3D semantic occupancy prediction performance of mIoU<sub>D</sub><sup>m</sup> and mIoU<sup>m</sup> w.r.t. training *with* camera visible mask on Occ3D. Here, \* denotes using radar points as additional inputs. The best overall results are highlighted in **bold**. The highest results from other methods are underscored, with improvements relative to these indicated by arrows. FPS is measured on RTX 4090.

ily include traffic-critical objects. Our method significantly outperforms existing approaches for both small-scale and large-scale image input sizes and image backbones.

## 3D Semantic Occupancy Prediction without Mask.

Tab. 2 presents the results of 3D semantic occupancy prediction without using the camera visible mask. Our method achieves the best performance in terms of RayIoU and mIoU. This demonstrates the effectiveness of our method in capturing the complete scene context and understanding the spatial relationships between objects. Our method also exhibits superior performance in terms of RayIoU at different distances, further highlighting its robustness in capturing object details. Notably, our method improves performance with minimal overhead. Our model not only leads in performance, but also shows significantly faster inference in its scaled-down version compared to similar methods, which is crucial for autonomous driving tasks.

**3D Semantic Occupancy and Flow Prediction.** Tab. 3 showcases the results of 3D semantic occupancy and flow prediction on the OpenOcc dataset. Our method achieves the best performance in terms of Occ Score, mAVE, mAVE<sub>TP</sub>, RayIoU, and RayIoU at different distances. This demonstrates the effectiveness of our method in capturing both semantic and motion information, highlighting its robustness in understanding the scene dynamics. AdaOcc-2D surpasses AdaOcc-3D in terms of mAVE and mAVE<sub>TP</sub>. This can be attributed to two factors: 1) mAVE<sub>TP</sub> are calculated on true positive areas, which means the number of ray queries to calculate the metric is influenced by the semantic

Method	Backbone	Input Size	mIoU	RayIoU	RayIoU <sub>1m, 2m, 4m</sub>			FPS
OccFormer [50]	ResNet-101	640 × 960	21.9	-	-	-	-	-
TPVFormer [11]	ResNet-101	640 × 960	27.8	-	-	-	-	-
CTF-Occ [38]	ResNet-101	640 × 960	28.5	-	-	-	-	-
BEVFormer [19]	ResNet-101	900×1600	23.7	32.4	26.1	32.9	38.0	4.4
BEVDetOcc-SOLO [10]	ResNet-50	256×704	24.3	35.2	31.2	35.9	38.4	6.5
FB-Occ [20]	ResNet-50	256×704	31.1	39.0	33.0	40.0	44.0	10.3
RenderOcc [34]	Swin-Base	512×1408	24.4	19.5	13.4	19.6	25.5	-
SparseOcc [24]	ResNet-50	256×704	30.9	36.1	30.2	36.8	41.2	15.0
Panoptic-FlashOcc [47]	ResNet-50	256×704	<u>31.6</u>	38.5	32.8	39.3	43.4	24.2
OPUS [40]	ResNet-50	256×704	-	<u>41.2</u>	34.7	42.1	46.7	8.2
<b>ALOcc-2D-mini</b>	ResNet-50	256×704	33.4	39.3	32.9	40.1	44.8	30.5
<b>ALOcc-2D</b>	ResNet-50	256×704	37.4 $\uparrow$ 5.8	43.0 $\uparrow$ 1.8	37.1	43.8	48.2	8.2
<b>ALOcc-3D</b>	ResNet-50	256×704	<b>38.0</b> $\uparrow$ 6.4	<b>43.7</b> $\uparrow$ 2.5	<b>37.8</b>	<b>44.7</b>	<b>48.8</b>	6.0

Table 2. 3D semantic occupancy prediction performance of RayIoU and mIoU w.r.t. training *without* camera visible mask on Occ3D. ALOcc-3D achieves the best performance, and ALOcc-2D-mini attains the best efficiency with strong performance.

Method	Backbone	Input Size	Occ Score	mAVE	mAVE <sub>TP</sub>	RayIoU	RayIoU <sub>1m, 2m, 4m</sub>		
OccNet [39]	ResNet-50	900×1600	35.7	-	1.61	39.66	29.3	39.7	50.0
OccNeRF [48]	ResNet-101	256×704	28.5	-	1.59	31.7	16.6	29.3	49.2
RenderOcc [34]	Swin-Base	512×1408	33.0	-	1.63	36.7	20.3	32.7	49.9
LetOccFlow [27]	ConvNeXt-Base	512×1408	36.4	-	1.45	<u>40.5</u>	25.5	39.7	56.3
BEVDetOcc-SOLO [10]	ResNet-50	250×704	33.0	1.42	1.78	36.7	31.6	37.3	41.1
FB-Occ [20]	ResNet-50	250×704	39.2	<u>0.591</u>	0.651	39.0	32.7	39.9	44.4
CascadeFlow [23]	ResNet-50	250×704	40.9	-	<u>0.47</u>	39.6	33.5	40.6	45.3
F-Occ [23]	FlashInternImage-Tiny	250×704	<u>41.0</u>	-	0.493	39.9	33.9	40.7	45.2
<b>ALOcc-Flow-2D</b>	ResNet-50	256×704	42.1 $\uparrow$ 1.1	<b>0.537</b> $\downarrow$ 0.054	<b>0.427</b> $\downarrow$ 0.043	40.5	34.3	41.3	45.8
<b>ALOcc-Flow-3D</b>	ResNet-50	256×704	<b>43.0</b> $\uparrow$ 2.0	0.556 $\downarrow$ 0.035	0.481	<b>41.9</b> $\uparrow$ 1.4	<b>35.6</b>	<b>42.8</b>	<b>47.4</b>

Table 3. 3D semantic occupancy and flow prediction performance on OpenOcc.

Condition	mIoU <sub>mD</sub>	mIoU <sub>m</sub>	mIoU	RayIoU	RayIoU <sub>1m, 2m, 4m</sub>		
0 ALOcc-2D-40	38.5	44.5	36.8	42.5	36.6	43.4	47.7
1 Exp#0-AL	37.5	43.5	36.1	41.3	35.2	42.1	46.6
2 Exp#0-SP	36.0	42.1	33.8	39.9	34.5	40.6	44.7
3 Exp#2-AL	34.9	41.2	33.3	39.5	34.0	40.3	44.2

Table 4. Ablation study on semantic occupancy prediction using Occ3D. **AL** and **SP** denote Adaptive Lifting and Semantic Prototype-based occupancy head, respectively.

prediction; 2) This benchmark calculates the flow on X and Y axes, so compressing the height and adding the channel focus more critical motion clues.

#### 4.4. Ablation Study

Unless specified, we use ALOcc-2D with a BEV feature channel of 40 as our baseline for these experiments.

**Components Analysis for Occ Head.** Tab. 4 presents an ablation study to evaluate the effectiveness of our core components in terms of semantic occupancy results. The full model (**Exp#0**) demonstrates superior performance across all metrics. Removing the adaptive lifting component (**Exp#1** and **Exp#3**) results in decreased performance, particularly in mIoU<sub>mD</sub> and mIoU, underscoring the efficacy of our adaptive and accurate 2D-to-3D view transformation. In **Exp#2**, we substitute the semantic prototype-based oc-

Condition	Occ Score	mAVE	mAVE <sub>TP</sub>	RayIoU	RayIoU <sub>1m, 2m, 4m</sub>		
0 ALOcc-2D-40	-	-	-	42.4	35.9	43.3	47.9
1 Exp#0+Flow	40.7	0.597	0.508	39.7	33.5	40.5	45.2
2 Exp#1+BC	39.9	0.565	0.464	38.3	32.7	39.0	43.3
3 Exp#1+CV	41.1	0.588	0.503	40.2	33.8	41.1	45.6
4 Exp#2+CV	41.1	0.562	0.451	39.6	33.3	40.4	45.1
5 Exp#4+CS	42.1	0.537	0.427	40.5	34.3	41.3	45.8

Table 5. Occupancy and flow prediction results w.r.t. different settings on OpenOcc. **Flow** represents flow head, **BC** denotes using bin classification, **CV** represents employing BEV cost volume, and **CS** is channel scaling up from 40 to 80.

cupancy head with FBOcc’s occupancy head, leading to a more pronounced performance decline. This observation highlights the crucial role of the SP component in enhancing the model’s semantic occupancy prediction accuracy.

**Components Analysis for Flow Head.** As shown in Tab. 5, we conducted an ablation study to evaluate how different components affect flow prediction performance. In **Exp#1**, we add a flow head implemented with a simple convolution. **Exp#1 vs. Exp#0** show that adding flow head harms the prediction of semantic occupancy. This is due to the motion flow containing different information from the semantic occupancy, which increases the burden of volume features. The results of **Exp#2 vs. Exp#1** show that using bin classification significantly improves flow prediction per-



formance. **Exp#3, #4** demonstrate that the use of BEV cost volume alleviates pressure on scene representation, enhancing flow prediction while maintaining occupancy prediction performance. In **Exp#5**, increasing BEV feature channels substantially improves overall performance, indicating that the information capacity of features is a bottleneck in joint learning of semantic occupancy and occupancy flow.

## 5. Conclusion

In this paper, we explore the challenge of vision-based 3D semantic occupancy and flow prediction. We propose an occlusion-aware adaptive lifting method, complemented by depth denoising to enhance the adaptability and robustness of the 2D-to-3D view transformation process. To further improve semantic occupancy learning, we introduce a semantic prototype-based occupancy head that aligns 2D and 3D semantics, combined with hard sample mining techniques to mitigate the long-tail problem. Additionally, we present a BEV cost volume-based approach to facilitate occupancy flow learning, reducing the burden on features to represent both semantics and flow simultaneously. Evaluations conducted on the Occ3D and OpenOcc datasets demonstrate that our method outperforms current SOTA solutions. Benefiting from the lightweight nature of our approach, we provide multiple model versions: our highest-performing model is faster than other methods with comparable performance, while our fastest model achieves superior performance compared to methods with similar speed.

## References

- [1] Jens Behley, Martin Garbade, Andres Milioto, Jan Quenzel, Sven Behnke, Cyrill Stachniss, and Jurgen Gall. Semantickitti: A dataset for semantic scene understanding of lidar sequences. In *Proceedings of the IEEE/CVF International Conference on Computer Vision*, pages 9297–9307, 2019. 2
- [2] Shariq Farooq Bhat, Ibraheem Alhashim, and Peter Wonka. Adabins: Depth estimation using adaptive bins. In *Proceedings of the IEEE/CVF Conference on Computer Vision and Pattern Recognition*, pages 4009–4018, 2021. 6
- [3] Holger Caesar, Varun Bankiti, Alex H Lang, Sourabh Vora, Venice Erin Liong, Qiang Xu, Anush Krishnan, Yu Pan, Giancarlo Baldan, and Oscar Beijbom. nuscenes: A multi-modal dataset for autonomous driving. In *Proceedings of the IEEE/CVF Conference on Computer Vision and Pattern Recognition*, pages 11621–11631, 2020. 6
- [4] Anh-Quan Cao and Raoul de Charette. Monoscene: Monocular 3d semantic scene completion. In *Proceedings of the IEEE/CVF Conference on Computer Vision and Pattern Recognition*, pages 3991–4001, 2022. 2
- [5] Xiaokang Chen, Kwan-Yee Lin, Chen Qian, Gang Zeng, and Hongsheng Li. 3d sketch-aware semantic scene completion via semi-supervised structure prior. In *Proceedings of the IEEE/CVF Conference on Computer Vision and Pattern Recognition*, pages 4193–4202, 2020. 2
- [6] Bowen Cheng, Ishan Misra, Alexander G Schwing, Alexander Kirillov, and Rohit Girdhar. Masked-attention mask transformer for universal image segmentation. In *Proceedings of the IEEE/CVF Conference on Computer Vision and Pattern Recognition*, pages 1290–1299, 2022. 2, 5
- [7] Kaiming He, Xiangyu Zhang, Shaoqing Ren, and Jian Sun. Deep residual learning for image recognition. In *Proceedings of the IEEE Conference on Computer Vision and Pattern Recognition*, pages 770–778, 2016. 6
- [8] Yulin He, Wei Chen, Tianci Xun, and Yusong Tan. Real-time 3d occupancy prediction via geometric-semantic disentanglement. *arXiv preprint arXiv:2407.13155*, 2024. 4
- [9] Jiawei Hou, Xiaoyan Li, Wenhao Guan, Gang Zhang, Di Feng, Yuheng Du, Xiangyang Xue, and Jian Pu. Fastocc: Accelerating 3d occupancy prediction by fusing the 2d bird’s-eye view and perspective view. In *IEEE International Conference on Robotics and Automation*, 2024. 7
- [10] Junjie Huang and Guan Huang. Bevdet4d: Exploit temporal cues in multi-camera 3d object detection. *arXiv preprint arXiv:2203.17054*, 2022. 1, 2, 3, 6, 7, 8
- [11] Yuanhui Huang, Wenzhao Zheng, Yunpeng Zhang, Jie Zhou, and Jiwen Lu. Tri-perspective view for vision-based 3d semantic occupancy prediction. *arXiv preprint arXiv:2302.07817*, 2023. 1, 2, 3, 8
- [12] Yuanhui Huang, Wenzhao Zheng, Borui Zhang, Jie Zhou, and Jiwen Lu. Selfocc: Self-supervised vision-based 3d occupancy prediction. In *Proceedings of the IEEE/CVF Conference on Computer Vision and Pattern Recognition*, pages 19946–19956, 2024. 3
- [13] Alexander Kirillov, Yuxin Wu, Kaiming He, and Ross Girshick. Pointrend: Image segmentation as rendering. In *Proceedings of the IEEE/CVF Conference on Computer Vision and Pattern Recognition*, pages 9799–9808, 2020. 5
- [14] Feng Li, Hao Zhang, Shilong Liu, Jian Guo, Lionel M Ni, and Lei Zhang. Dn-detr: Accelerate detr training by introducing query denoising. In *Proceedings of the IEEE/CVF Conference on Computer Vision and Pattern Recognition*, pages 13619–13627, 2022. 4
- [15] Jie Li, Yu Liu, Dong Gong, Qinfeng Shi, Xia Yuan, Chunxia Zhao, and Ian Reid. Rgb-d based dimensional decomposition residual network for 3d semantic scene completion. In *Proceedings of the IEEE/CVF Conference on Computer Vision and Pattern Recognition*, pages 7693–7702, 2019. 2
- [16] Jinke Li, Xiao He, Chonghua Zhou, Xiaoqiang Cheng, Yang Wen, and Dan Zhang. Viewformer: Exploring spatiotemporal modeling for multi-view 3d occupancy perception via view-guided transformers. In *Computer Vision—ECCV 2024: 18th European Conference*, 2024. 3, 7
- [17] Yinhao Li, Han Bao, Zheng Ge, Jinrong Yang, Jianjian Sun, and Zeming Li. Bevestereo: Enhancing depth estimation in multi-view 3d object detection with temporal stereo. In *Proceedings of the AAAI Conference on Artificial Intelligence*, pages 1486–1494, 2023. 1, 2, 3
- [18] Yiming Li, Zhiding Yu, Christopher Choy, Chaowei Xiao, Jose M Alvarez, Sanja Fidler, Chen Feng, and Anima Anand-

- kumar. Voxformer: Sparse voxel transformer for camera-based 3d semantic scene completion. In *Proceedings of the IEEE/CVF Conference on Computer Vision and Pattern Recognition*, pages 9087–9098, 2023. 2, 7
- [19] Zhiqi Li, Wenhao Wang, Hongyang Li, Enze Xie, Chonghao Sima, Tong Lu, Qiao Yu, and Jifeng Dai. Bevformer: Learning bird’s-eye-view representation from multi-camera images via spatiotemporal transformers. *arXiv preprint arXiv:2203.17270*, 2022. 1, 2, 7, 8
- [20] Zhiqi Li, Zhiding Yu, David Austin, Mingsheng Fang, Shiyi Lan, Jan Kautz, and Jose M Alvarez. Fb-occ: 3d occupancy prediction based on forward-backward view transformation. *arXiv preprint arXiv:2307.01492*, 2023. 3, 6, 7, 8
- [21] Zhiqi Li, Zhiding Yu, Wenhao Wang, Anima Anandkumar, Tong Lu, and Jose M Alvarez. Fb-bev: Bev representation from forward-backward view transformations. In *Proceedings of the IEEE/CVF International Conference on Computer Vision*, pages 6919–6928, 2023. 2, 6
- [22] Zhenyu Li, Xuyang Wang, Xianming Liu, and Junjun Jiang. Binsformer: Revisiting adaptive bins for monocular depth estimation. *IEEE Transactions on Image Processing*, 2024. 6
- [23] Zhimin Liao and Ping Wei. Cascadeflow: 3d occupancy and flow prediction with cascaded sparsity sampling refinement framework. *CVPR 2024 Autonomous Grand Challenge Track On Occupancy and Flow*, 2024. 8
- [24] Haisong Liu, Haiguang Wang, Yang Chen, Zetong Yang, Jia Zeng, Li Chen, and Limin Wang. Fully sparse 3d occupancy prediction. In *Computer Vision—ECCV 2024: 18th European Conference*, 2024. 3, 6, 8
- [25] Lizhe Liu, Bohua Wang, Hongwei Xie, Daqi Liu, Li Liu, Zhiqiang Tian, Kuiyuan Yang, and Bing Wang. Surroundsdf: Implicit 3d scene understanding based on signed distance field. In *Proceedings of the IEEE/CVF Conference on Computer Vision and Pattern Recognition*, 2024. 7
- [26] Shice Liu, Yu Hu, Yiming Zeng, Qiankun Tang, Beibei Jin, Yinhe Han, and Xiaowei Li. See and think: Disentangling semantic scene completion. *Advances in Neural Information Processing Systems*, 31, 2018. 2
- [27] Yili Liu, Linzhan Mou, Xuan Yu, Chenrui Han, Sitong Mao, Rong Xiong, and Yue Wang. Let occ flow: Self-supervised 3d occupancy flow prediction. *arXiv preprint arXiv:2407.07587*, 2024. 3, 8
- [28] Ze Liu, Yutong Lin, Yue Cao, Han Hu, Yixuan Wei, Zheng Zhang, Stephen Lin, and Baining Guo. Swin transformer: Hierarchical vision transformer using shifted windows. In *Proceedings of the IEEE/CVF International Conference on Computer Vision (ICCV)*, 2021. 6
- [29] Ilya Loshchilov and Frank Hutter. Fixing weight decay regularization in adam. 2018. 7
- [30] Yuhang Lu, Xinge Zhu, Tai Wang, and Yuexin Ma. Octreeocc: Efficient and multi-granularity occupancy prediction using octree queries. *arXiv preprint arXiv:2312.03774*, 2023. 3
- [31] Junyi Ma, Xieyuanli Chen, Jiawei Huang, Jingyi Xu, Zhen Luo, Jintao Xu, Weihao Gu, Rui Ai, and Hesheng Wang. Cam4docc: Benchmark for camera-only 4d occupancy forecasting in autonomous driving applications. In *Proceedings of the IEEE/CVF Conference on Computer Vision and Pattern Recognition*, pages 21486–21495, 2024. 1
- [32] Qihang Ma, Xin Tan, Yanyun Qu, Lizhuang Ma, Zhizhong Zhang, and Yuan Xie. Cotr: Compact occupancy transformer for vision-based 3d occupancy prediction. *arXiv preprint arXiv:2312.01919*, 2023. 3, 7
- [33] Mingjie Pan, Li Liu, Jiaming Liu, Peixiang Huang, Longlong Wang, Shanghang Zhang, Shaoqing Xu, Zhiyi Lai, and Kuiyuan Yang. Uniocc: Unifying vision-centric 3d occupancy prediction with geometric and semantic rendering. *arXiv preprint arXiv:2306.09117*, 2023. 7
- [34] Mingjie Pan, Jiaming Liu, Renrui Zhang, Peixiang Huang, Xiaoqi Li, Hongwei Xie, Bing Wang, Li Liu, and Shanghang Zhang. Renderocc: Vision-centric 3d occupancy prediction with 2d rendering supervision. In *2024 IEEE International Conference on Robotics and Automation (ICRA)*, pages 12404–12411. IEEE, 2024. 3, 8
- [35] Jinhyung Park, Chenfeng Xu, Shijia Yang, Kurt Keutzer, Kris Kitani, Masayoshi Tomizuka, and Wei Zhan. Time will tell: New outlooks and a baseline for temporal multi-view 3d object detection. *arXiv preprint arXiv:2210.02443*, 2022. 6
- [36] Jonah Philion and Sanja Fidler. Lift, splat, shoot: Encoding images from arbitrary camera rigs by implicitly unprojecting to 3d. In *Computer Vision—ECCV 2020: 16th European Conference, Glasgow, UK, August 23–28, 2020, Proceedings, Part XIV 16*, pages 194–210. Springer, 2020. 2, 3
- [37] Yiang Shi, Tianheng Cheng, Qian Zhang, Wenyu Liu, and Xinggang Wang. Occupancy as set of points. In *Computer Vision—ECCV 2024: 18th European Conference*, 2024. 6, 7
- [38] Xiaoyu Tian, Tao Jiang, Longfei Yun, Yucheng Mao, Huitong Yang, Yue Wang, Yilun Wang, and Hang Zhao. Occ3d: A large-scale 3d occupancy prediction benchmark for autonomous driving. *Advances in Neural Information Processing Systems*, 36, 2024. 1, 2, 3, 6, 8
- [39] Wenwen Tong, Chonghao Sima, Tai Wang, Li Chen, Silei Wu, Hanming Deng, Yi Gu, Lewei Lu, Ping Luo, Dahua Lin, et al. Scene as occupancy. In *Proceedings of the IEEE/CVF International Conference on Computer Vision*, pages 8406–8415, 2023. 1, 2, 3, 6, 8
- [40] Jiabao Wang, Zhaojiang Liu, Qiang Meng, Liujiang Yan, Ke Wang, Jie Yang, Wei Liu, Qibin Hou, and Mingming Cheng. Opus: occupancy prediction using a sparse set. In *Advances in Neural Information Processing Systems*, 2024. 3, 7, 8
- [41] Xiaofeng Wang, Zheng Zhu, Wenbo Xu, Yunpeng Zhang, Yi Wei, Xu Chi, Yun Ye, Dalong Du, Jiwen Lu, and Xinggang Wang. Openoccupancy: A large scale benchmark for surrounding semantic occupancy perception. *arXiv preprint arXiv:2303.03991*, 2023. 1, 3
- [42] Yuqi Wang, Yuntao Chen, Xingyu Liao, Lue Fan, and Zhaoxiang Zhang. Panoocc: Unified occupancy representation for camera-based 3d panoptic segmentation. In *Proceedings of the IEEE/CVF Conference on Computer Vision and Pattern Recognition*, 2024. 3, 6, 7
- [43] Yi Wei, Linqing Zhao, Wenzhao Zheng, Zheng Zhu, Jie Zhou, and Jiwen Lu. Surroundocc: Multi-camera 3d occupancy prediction for autonomous driving. *arXiv preprint arXiv:2303.09551*, 2023. 3, 7

- [44] Philipp Wolters, Johannes Gilg, Torben Teepe, Fabian Herzog, Anouar Laouichi, Martin Hofmann, and Gerhard Rigoll. Unleashing hydra: Hybrid fusion, depth consistency and radar for unified 3d perception. *arXiv preprint arXiv:2403.07746*, 2024. 7
- [45] Shichao Yang, Yulan Huang, and Sebastian Scherer. Semantic 3d occupancy mapping through efficient high order crfs. In *2017 IEEE/RSJ International Conference on Intelligent Robots and Systems (IROS)*, pages 590–597. IEEE, 2017. 1
- [46] Zichen Yu, Changyong Shu, Jiajun Deng, Kangjie Lu, Zongdai Liu, Jiangyong Yu, Dawei Yang, Hui Li, and Yan Chen. Flashocc: Fast and memory-efficient occupancy prediction via channel-to-height plugin. *arXiv preprint arXiv:2311.12058*, 2023. 7
- [47] Zichen Yu, Changyong Shu, Qianpu Sun, Junjie Linghu, Xiaobao Wei, Jiangyong Yu, Zongdai Liu, Dawei Yang, Hui Li, and Yan Chen. Panoptic-flashocc: An efficient baseline to marry semantic occupancy with panoptic via instance center. *arXiv preprint arXiv:2406.10527*, 2024. 8
- [48] Chubin Zhang, Juncheng Yan, Yi Wei, Jiaxin Li, Li Liu, Yansong Tang, Yueqi Duan, and Jiwen Lu. Occnerf: Self-supervised multi-camera occupancy prediction with neural radiance fields. *arXiv preprint arXiv:2312.09243*, 2023. 3, 8
- [49] Hao Zhang, Feng Li, Shilong Liu, Lei Zhang, Hang Su, Jun Zhu, Lionel M Ni, and Heung-Yeung Shum. Dino: Detr with improved denoising anchor boxes for end-to-end object detection. *arXiv preprint arXiv:2203.03605*, 2022. 4
- [50] Yunpeng Zhang, Zheng Zhu, and Dalong Du. Occformer: Dual-path transformer for vision-based 3d semantic occupancy prediction. *arXiv preprint arXiv:2304.05316*, 2023. 2, 5, 8